AFRL-AFOSR-UK-TR-2014-0010

Laterally-biased quantum IR detectors

Alvaro de Guzman Fernandez

Universidad Politecnica de Madrid
Instituto de Sistemas Optoelectronicos y Microtecnologia
Calle Ramiro de Maeztu 7
Madrid 28040 SPAIN

EOARD Grant 12-3006

Report Date: October 2013

Final Report from 15 October 2011 to 14 October 2013

Air Force Research Laboratory
Air Force Office of Scientific Research
European Office of Aerospace Research and Development
Unit 4515, APO AE 09421-4515

REPORT DOCUMENTATION PAGE

Form Approved OMB No. 0704-0188

1. REPORT DATE *(DD-MM-YYYY)*	2. REPORT TYPE	3. DATES COVERED *(From – To)*
23 October 2013	Final Report	15 October 2011 – 14 October 2013

4. TITLE AND SUBTITLE

Laterally-biased quantum IR detectors

5a. CONTRACT NUMBER

FA8655-12-1-3006

5b. GRANT NUMBER

Grant 12-3006

5c. PROGRAM ELEMENT NUMBER

61102F

6. AUTHOR(S)

Alvaro de Guzman Fernandez

5d. PROJECT NUMBER

5d. TASK NUMBER

5e. WORK UNIT NUMBER

7. PERFORMING ORGANIZATION NAME(S) AND ADDRESS(ES)
Universidad Politecnica de Madrid
Instituto de Sistemas Optoelectronicos y Microtecnologia
Calle Ramiro de Maeztu 7
Madrid 28040 SPAIN

8. PERFORMING ORGANIZATION REPORT NUMBER

N/A

9. SPONSORING/MONITORING AGENCY NAME(S) AND ADDRESS(ES)

EOARD
Unit 4515
APO AE 09421-4515

10. SPONSOR/MONITOR'S ACRONYM(S)

AFRL/AFOSR/IOE (EOARD)

11. SPONSOR/MONITOR'S REPORT NUMBER(S)

AFRL-AFOSR-UK-TR-2014-0010

12. DISTRIBUTION/AVAILABILITY STATEMENT

Distribution A: Approved for public release; distribution is unlimited.

13. SUPPLEMENTARY NOTES

14. ABSTRACT

This project was aimed to the development of a suitable fabrication system to produce laterally-biased quantum well detectors with low dark current at room temperature. The development of quantum IR detectors with low dark current and operating at room temperature was achieved. On the one hand, we were able to reduce the dark current by biasing the pinch-off gates/lateral contacts in reverse way. In addition, we were able to etched the quantum wells (QWs) to avoid direct conduction and only the photo generated carriers are expected to reach the lateral contacts. In this case, the growth of more than 2 QWs is possible, thus, the responsivity could be enhanced. It has been demonstrated that this technology is very promising for the development of single QWIP detectors working at high temperature. The main objectives achieved can be summarized as follows:
1. Development of a ion beam etching chamber to be connected to the main MBE system. This objective was successfully achieved.
2. Optimization of the etching and post-growth processes in terms of surface quality. The samples were fabricated by alternate etching and growth steps.
The QW surface quality was demonstrated to be high enough, with RMS roughness similar to that of the bare substrates.
3. Fabrication of structure I for RT operation. We have demonstrated RT response for MES-FET structures.

15. SUBJECT TERMS

EOARD, IR Detector, Materials, Electronic Materials, Quantum Well

16. SECURITY CLASSIFICATION OF:			17. LIMITATION OF ABSTRACT	18, NUMBER OF PAGES	19a. NAME OF RESPONSIBLE PERSON
a. REPORT	b. ABSTRACT	c. THIS PAGE			John Gonglewski
UNCLAS	UNCLAS	UNCLAS	SAR	27	19b. TELEPHONE NUMBER *(Include area code)* +44 (0)1895 616007

EOARD - Award No. FA8655-12-1-3006

Instituto de Sistemas Optoelectrónicos y Microtecnología (ISOM), Universidad Politécnica de Madrid

Laterally-biased quantum IR detectors

PI : Álvaro de Guzmán Fernández

Report of the period:

April 2013 - November 2013

Final Report

Álvaro de Guzmán Fernández

Raquel Gargallo Caballero

María José Milla

Table of contents

Laterally-biased quantum IR detectors

List of figures

Laterally biased quantum IR detectors

1. Introduction and previous work

The development of quantum IR detectors with low dark current and operating at room temperature is the main objective of this project. As shown in fig 1, two different structures were designed and studied in order to achieve this goal [1]. On the one hand, structure I is able to reduce the dark current by biasing the pinch-off gates/lateral contacts in reverse way. In structure II, the etching of the quantum wells (QWs) avoids the direct conduction and only the photogenerated carriers are expected to reach the lateral contacts. In this case, the growth of more than 2 QWs is possible, thus, the responsivity could be enhanced.

During the period corresponding to this report, our main goal was to reduce the thickness of the QWs of the lateral biased IR photodetectors in order to achieve operating wavelengths between 8 and 12 µm. In previous work, we demonstrated the viability of both structures to achieve very low dark currents and IR light detection at room temperature (RT). In the case of structure I, optical absorption at 9.5 µm was demonstrated in agreement with the calculations [2]. Moreover, we obtained a photocurrent peak at 21 µm at RT for structure II, also in good agreement with the simulations. During this last period we mainly focused on structure II. Our work aimed to fabricate and characterize a lateral bias quantum IR detector based on structure I, complying with the design requirements.

Regarding structure I, we modified the cleaning procedure after the ion implantation in order to improve the crystal quality of the material regrown. We processed and characterized a new sample as a photodetector following this improved method.

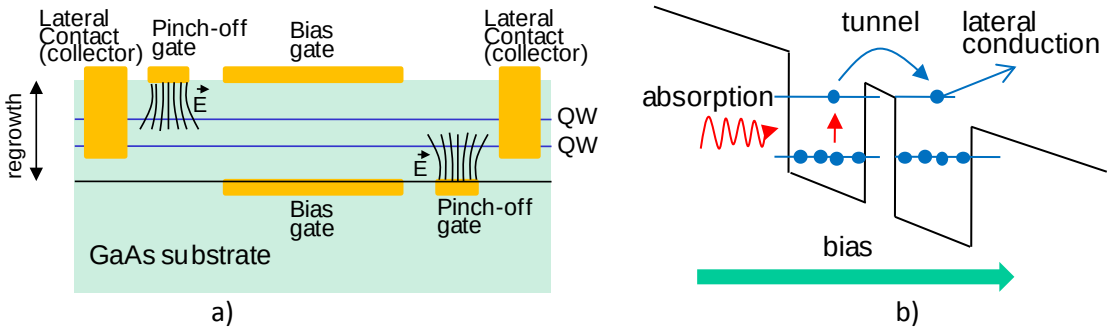

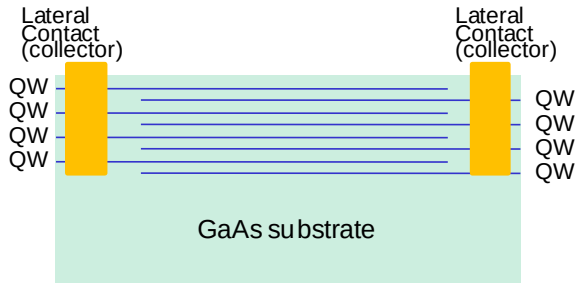

c)

FIG. 1 Quantum Structures for Tunable Detectors. a) Structure I, b) potential profile of structure I, c) Structure II

2. Procedures: Structure I

As already mentioned in previous reports concerning structure I, the creation of p-n junctions between the pinch off gates and the lateral contacts allows to obtain depletion layers at the sides of the well when they are reversed bias [3]. The buried p-type region was made by ion implantation of Zn ions prior to the growth step. In the case of the top p-type region, they were grown by MBE. The final structure of this device is depicted in fig. 2:

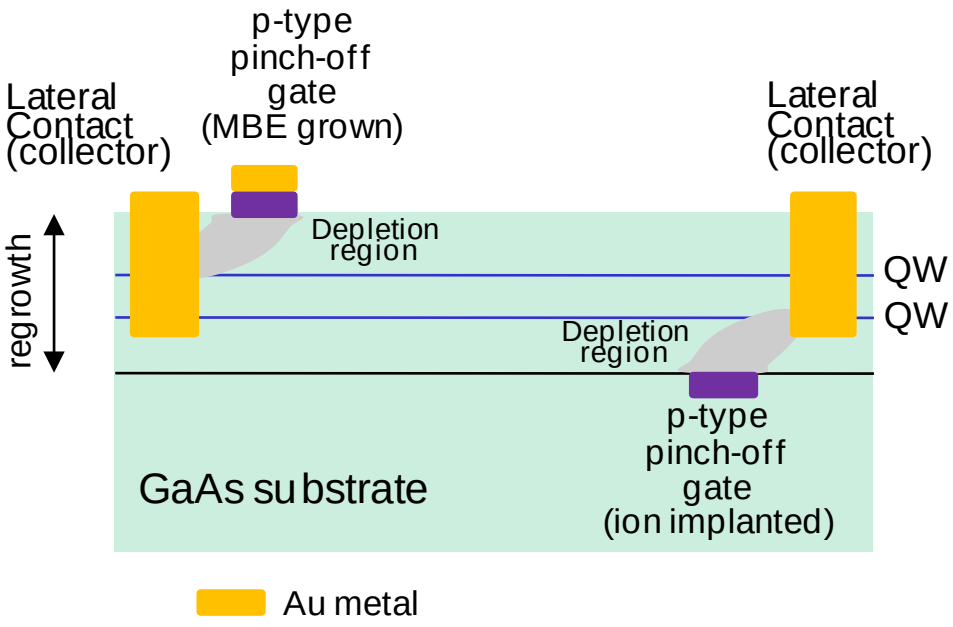

Fig. 2. Device with two quantum wells and p-type doping in the pinch-off gates.

The samples were implanted at LEONARD KROKO, INC. 2822-D WALNUT AVENUE, TUSTIN (CA), 92780 USA. We sent four 2'' wafers to be processed with the following parameters:

Energy	Dose (cm^{-2})	Rp (nm)	Concentration at Rp (cm^{-3})

180 KeV	$9.35 \cdot 10^{-11}$	83.7	$1 \cdot 10^{17}$
180 KeV	$9.35 \cdot 10^{-12}$	83.7	$1 \cdot 10^{18}$
350 KeV	$1.65 \cdot 10^{-12}$	163	$1 \cdot 10^{17}$
350 KeV	$1.65 \cdot 10^{-13}$	163	$1 \cdot 10^{18}$

Fig. 3 shows the different steps to develop the final device and a detail of the bottom contacts in the third dimension of the processing structure.

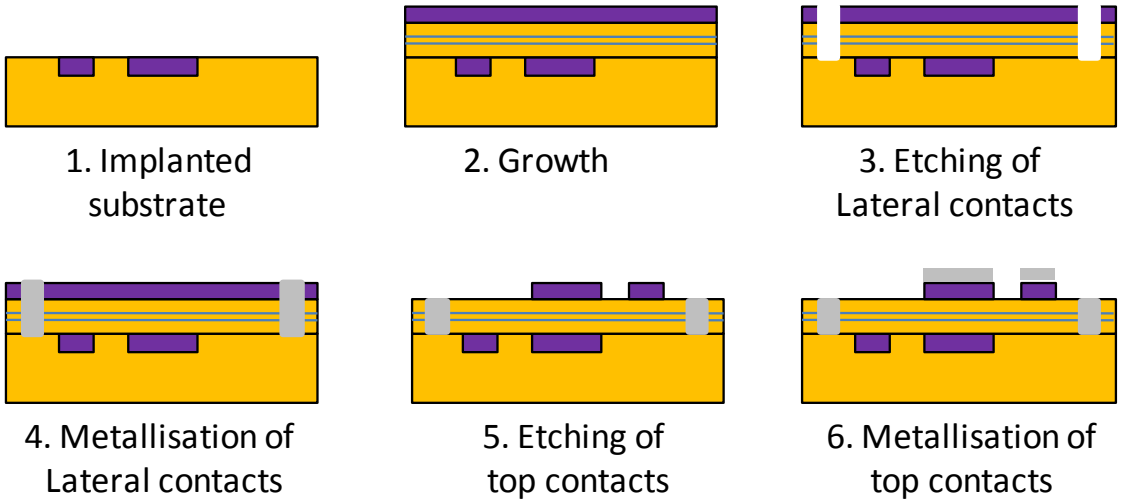

a)

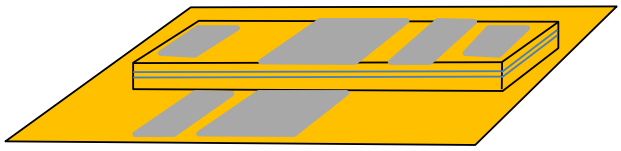

b)

Fig. 3 a) Processing steps of the device (magenta areas are p-type doping). b) Detail of the bottom contacts in the third dimension of the processing structure.

In the previous report, we obtained very high resistance values between lateral contacts without the application of a bias voltage to the pinch-off contacts. One possible explanation for these results is a low quality of the grown sample. The RHEED pattern during the growth

was spotty and the external look of this sample was clearly whitish. This could be attributed to the presence of resist remains even after the previous cleaning to the regrowth step. To face this problem, an extra step was incorporated to the standard cleaning procedure (consisting of the immersion of the sample in acetone): an etching step of the surface of the sample with an O_2 plasma. This new cleaning procedure has led to a streaky RHEED patterns and also a very good external look of the sample.

Afterwards, we measured the I-V characteristics of the detector between the lateral contacts, so that the pinch-off gates were left without connection. According to the characteristics, dimensions and doping concentration of the QWs, we would expect to obtain a resistance of around 20 KΩ.

As seen in fig. 4, the I-V characteristics demonstrated that the lateral contacts are ohmic and the resistance value between these contacts is around 30 MΩ.

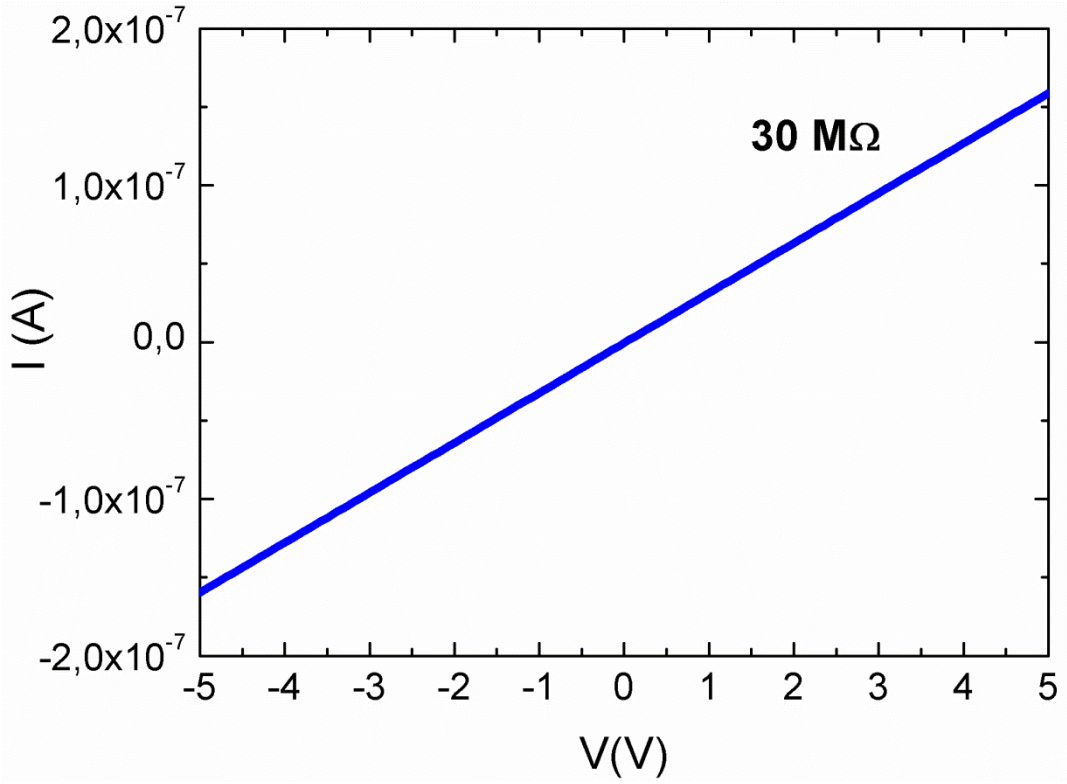

Fig. 4 I-V characteristic of the photodetector.

The experimental resistance value is still very high compared to the theoretical one. We checked by Nomarski microscopy the appearance of the surface after the processing steps (see fig. 5), and we did not find a homogeneous surface, but the presence of unidentified material remains on the surface of the sample. Despite the improvement of the resist removal procedure after the ion implantation, it is probably that some resist remains were still present, so that the later processing of the sample was not as homogeneous as we expected.

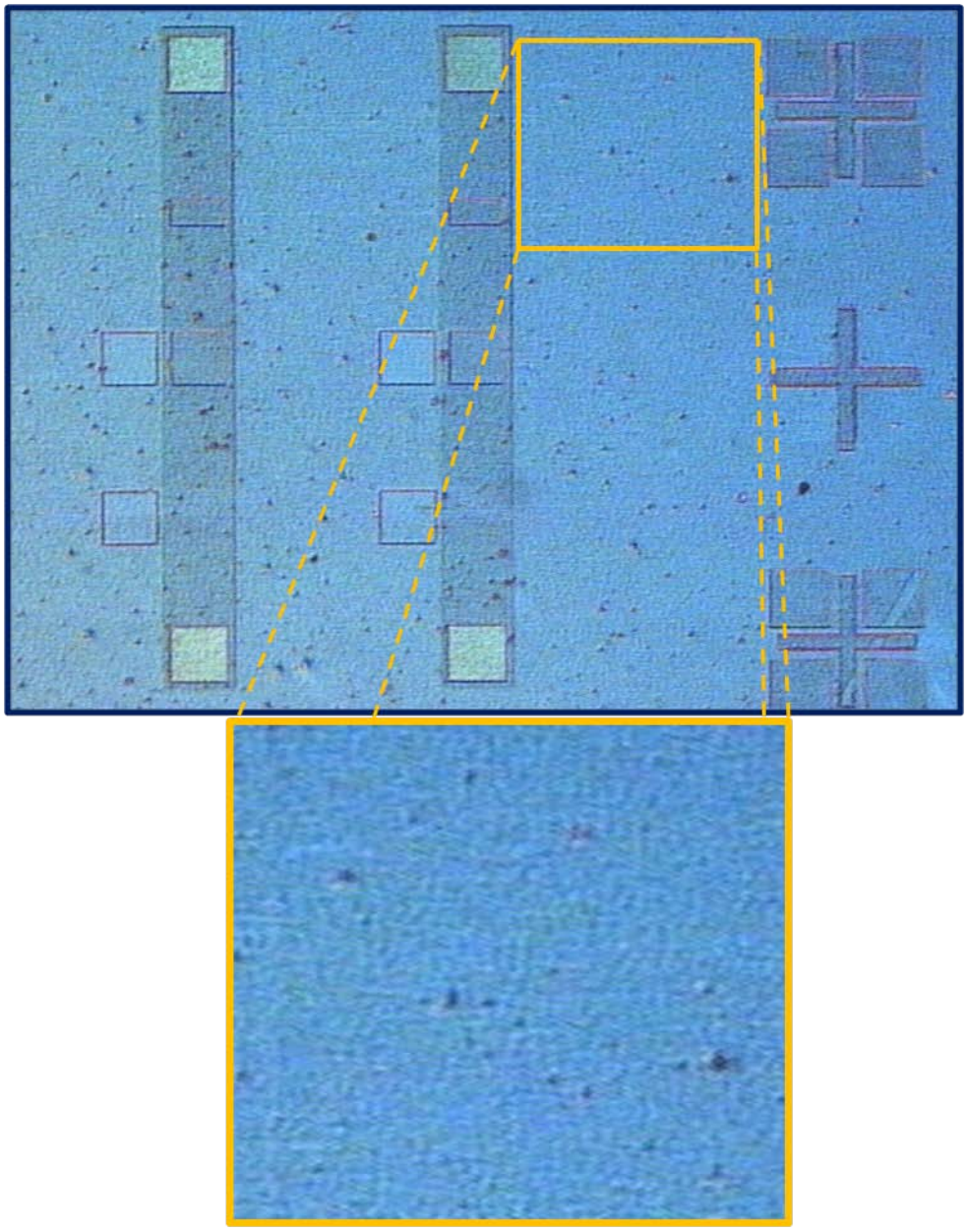

Fig.5 Nomarski image of the sample processed as a photodetector with structure I (top) and a detail of the bottom etched surface (bottom).

Thus, the high resistance value could be explained by this low quality of the surface after the sample processing. Hence, the optimization of the cleaning step before the regrowth procedure is clearly the key to achieve the successful development of structure I.

3. Procedures: Structure II

3.1 Summary of ion etching chamber assembly

To develop structure II, an Ar ion gun (IQE 12/38) was installed in a vacuum chamber connected to the MBE growth chamber in order to etch the edge of the QWs after their growth (see fig. 6). Therefore, we avoid the extraction of the sample from the vacuum environment when growth and etching processes are alternated. The whole fabrication of structure II can be performed without contamination risks.

a)

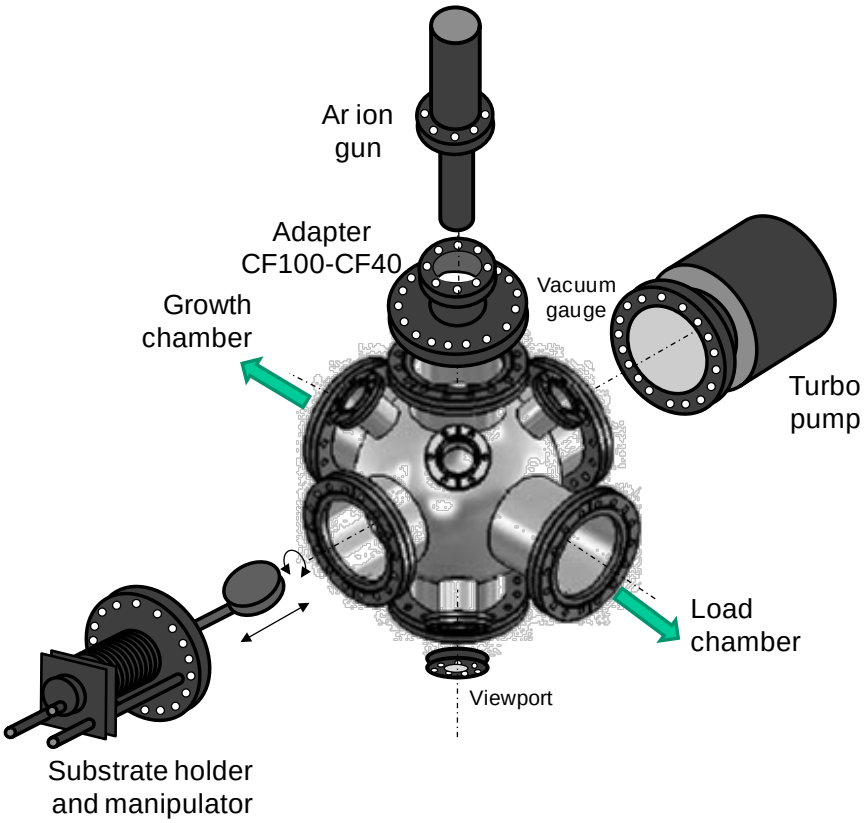

b)

Fig. 6 a) Ion gun IQE 12/38.
b) Etching chamber connected to the MBE growth system.

3.2 Design requirements: optimum etching conditions

In the previous report, we performed lateral biased IR photodetectors based on structure II with QWs thickness of 20 nm and barriers of 100 nm. Now, we want to reduce the QW thickness to values around 5 nm, and the barriers between 5 and 10 nm thick (see fig. 7).

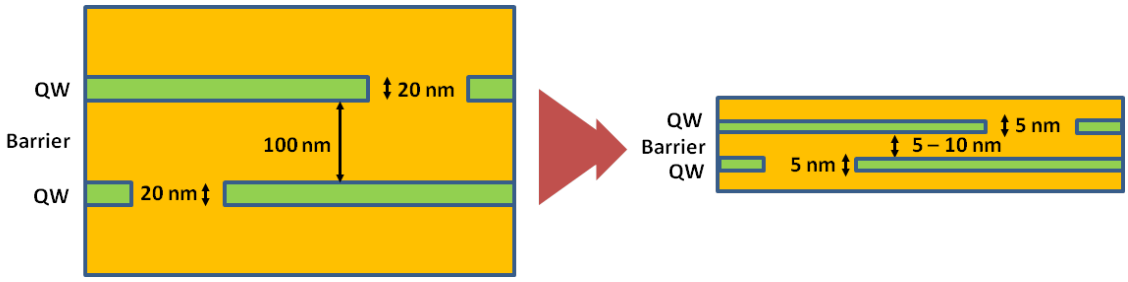

Fig. 7 Reduction of the QW and barrier thickness to values of 5 nm and 5 – 10 nm, respectively.

The fabrication of such structure II entails that the ion etching process fulfills two main design requirements: an accurate etching process and a surface quality similar to that of the native substrate.

- We need an ion sputtering accuracy of the order of at least the thickness of the QW. This accuracy will be closely related to the sputtering rate. In particular, we need to etch QWs of 5 nm all around an area of 2 x 10 mm. Thus, the etching rate should be of the order of a few nm/s.

- The roughness of the etched surface should be low enough to continue the correct fabrication process, so that the regrowth of a homogeneous material of a good quality is allowed.

The characteristics of the etching process depend on a set of parameters which can be adjusted through the power unit of the ion gun (fig. 8): energy, pressure, emission current, extractor, focus and geometrical distances and angles.

Fig. 8 Power supply of the Ar ion gun IQE 12/38.

In order to fulfill the above design requirements of structure II, the optimization of these parameters were addressed in the previous report. After several studies changing the etching

conditions, we found that a precise control of the etching rate and a good quality of the resulting etched surface were possible using the following set of parameters:

- Energy: 2000 V
- Pressure: 4e-7 Torr
- Emission current: 5 mA
- Extractor: 88.9%
- Focus: 76%
- Geometrical distance (from deflection plates to the sample): 44.4 mm

Afterwards, we performed an equivalent etching process to the one performed later for the fabrication of structure II using the optimized set of parameters. As shown in fig. 9, the layout of this etching consists of two areas of 2 x 10 mm of a few nm of depth, separated 1 mm. This separation distance between areas is the length of the active region where the excited electrons are able to tune out from one QW to the other one. The correct alignment of these two areas is essential. For this purpose, we installed a TV camera on one of the viewports of the etching chamber, together with a TV screen as an alignment set-up. Thereby, the drawing of several marks on the TV screen allows the accurate positioning of the substrate holder always at the same position (see the previous report for a detailed explanation).

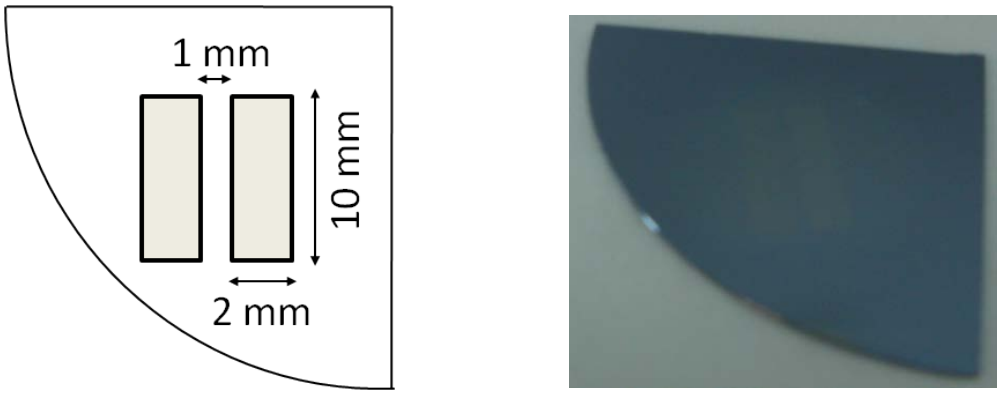

Fig. 9 a) Layout of a sample with two sputtered areas of 2 x 10 mm of 10 nm of depth, and b) image of the resulting surface after the etching process.

To study the etching accuracy and the surface morphology after the process, Atomic Force Microscopy (AFM) and profiler measurements were carried out.

First, as seen in the profiler measurements of fig. 10, the precision of the ion sputtering is of the order of nm. Additionally, the same results were obtained from the measurements performed at different position around the etched areas. Hence, the etching process was accurate enough to etch a QW with a thickness of 5 nm, and also in a homogeneous way. Subsequently, the quality of the etched surface was assessed. As first approach, we used the Alpha-Step profiler to extract at the scale of mm the maximum RMS roughness. A very good quality surface was observed (RMS roughness of 0.545 nm), almost comparable to the roughness of a native wafer (0.283 nm).

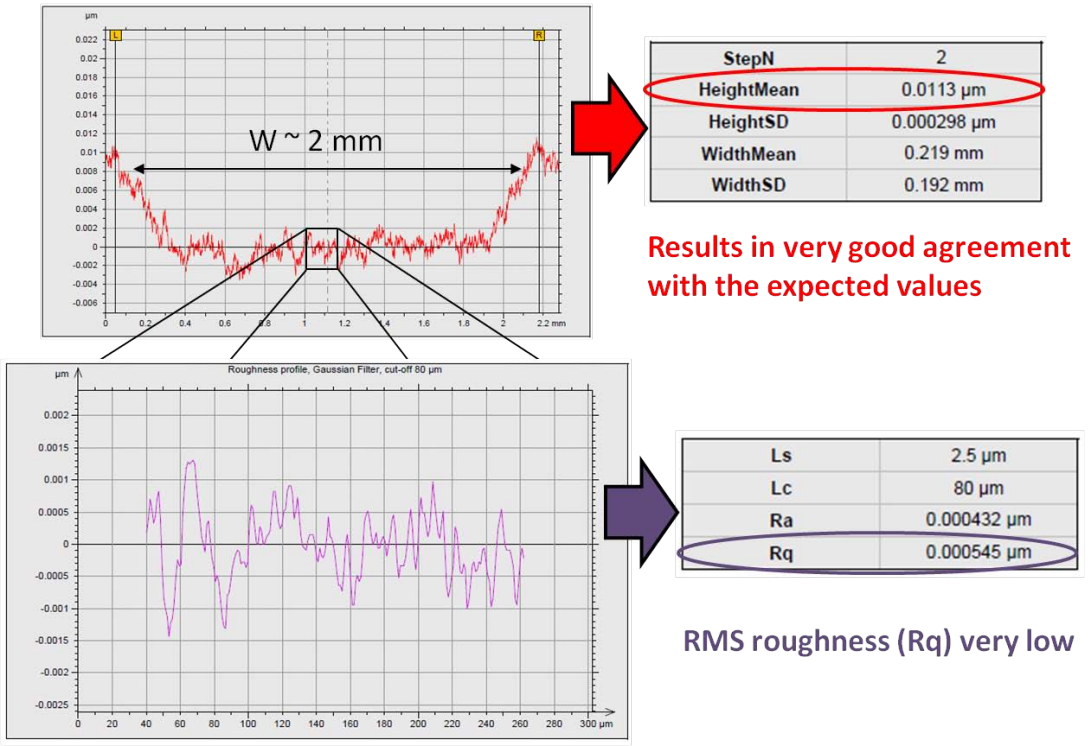

Fig. 10 Depth profile of one of the etched areas of 2 x10 mm. The results yield a homogeneous etching depth of 10 nm. The maximum RMS roughness obtained at high scale (of the order of mm) was 0.545 nm.

In order to perform a morphological analysis at a lower scale, AFM measurements of the etched surface were carried out. As shown in fig. 11, a RMS roughness of 0.277 nm was revealed, indicating very smooth surfaces after ion sputtering. As a consequence, we can state that the morphological quality of the surface after the etching process is comparable to that of the native substrate.

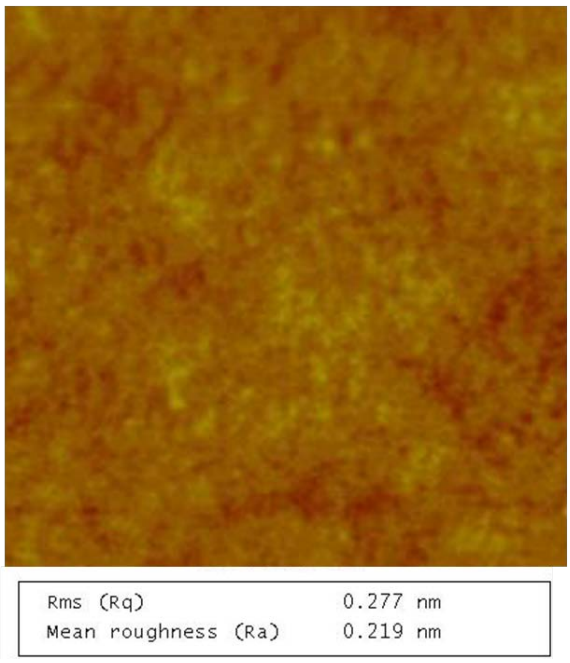

Fig. 11 500 nm x 500 nm AFM image of the etched surface using optimum etching conditions.

3.3 Fabrication of the structure

Once the etching parameters are mastered and etching process fulfills the structure II design requirements, we proceed to the fabrication of the lateral bias IR photodetector. In particular, as already mentioned, we want to grow thinner QWs (5 nm) and barriers (5 – 10 nm). The objective of such a thickness reduction is twofold: on the one hand, the improvement of the absorption, since the confinement of the excited levels is reduced; and on the other hand, the enhancement of the carrier transport due to the presence of thinner tunnel barriers.

In particular, we developed two different samples with structure II which basically differ in the thickness of the barrier. This will allow us to study later the effect of the barrier thickness both, on the structural characteristics of the regrown material and also on the operation of the IR photodetector.

- Sample A: It consists of 2 GaAs QWs of 5 nm separated by $Al_{0.3}Ga_{0.7}As$ barriers of 10 nm.
- Sample B: It consists of 2 GaAs QWs of 5 nm separated by $Al_{0.3}Ga_{0.7}As$ barriers of 5 nm.

Both types of samples were grown on undoped GaAs (100) substrates and were capped with a 10 nm-thick GaAs layer to avoid the oxidation of the top AlGaAs layer. The QWs were heavily Si-doped GaAs with a concentration of $2 \cdot 10^{18}$ cm^{-3}. Fig. 12 shows the particular structure of these samples.

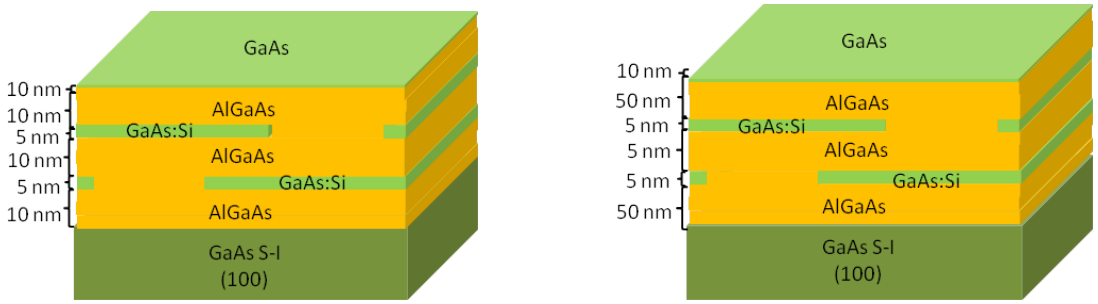

Fig. 12 Structure of the samples A (left) and B (right) based on "structure II".

Scanning Electron Microscopy was used to make a cross-sectional analysis of the samples. In the previous report, QWs of structure II were separated between them by large AlGaAs barriers (100 nm-thick), making possible the observation of the actual extension of the etching processes. By contrast, in these samples (A and B), the barrier between QWs is quite smaller, and thus the observation of the different QWs and the etching extension by SEM was not possible. However, as will be mentioned later, indirect measurements can provide this relevant information (section 3.5.2).

To develop this structure, we followed the steps detailed in fig. 13:

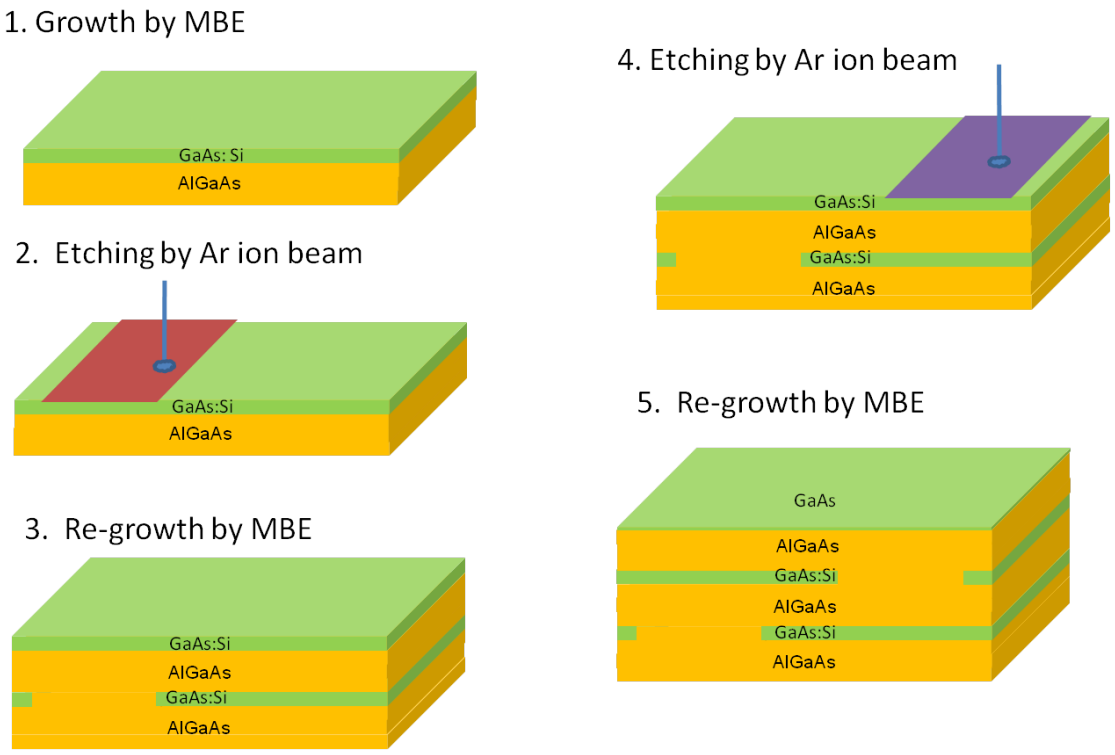

Fig. 13 Steps in the fabrication of the samples A and B.

First, we must grow the bottom AlGaAs barrier and bottom QW. Then, sample is transfer to the etching chamber and the edge of the QW is sputtered. Afterwards, sample is transfer again to the MBE growth chamber, and AlGaAs barrier and top QW are grown. Later, a second sputtering process is carried out in order to etch the edge of this second QW. And lastly, the rest of growth (top AlGaAs layer and GaAs capping layer) is completed in the growth chamber. Sample A and B were grown under optimized growth conditions which were the same used for the growth of the structure II in the previous report: GaAs and AlGaAs were grown at 580ºC and 600ºC, respectively, and using a III-V Beam Equivalent Pressure ratio of 25.

3.4 Morphological characterization

3.4.1 External look

At first glance, both samples (A and B) show an excellent appearance, i.e. flat and specular surfaces, which is in good agreement with the streaky RHEED pattern observed during the whole growth. Fig. 14 shows the external look of the Sample B.

Fig. 14. External look of Sample B after the fabrication process.

3.4.2 AFM measurements

We also performed AFM characterization of the surface of the samples after their fabrication process in order to analyze their morphology and structural quality at low scale. In this way, we can extract precise information about the regrowth process on the previously etched surfaces.

Despite the smooth and flat surfaces obtained after the etching step (see fig. 7) with comparable RMS roughness to that of the native substrate, AFM images revealed that the crystal quality during the regrowth is decreased. As seen in fig. 15 and fig. 16, such degradation is mainly due to the appearance of holes which were not apparently present in the sputtered surface. However, we found that the roughness of the regrown surface between holes (0.327-0.357 nm) is barely higher than that of the etched one (0.277 nm).

During sputtering process, Ar ion bombardment might be giving rise to the formation of pits [4] which act as nucleation sites during the later regrowth process leading to the formation of these holes in the surface. For this reason, we would expect that as the thickness of the regrown layer increases the depth of the holes also increases. We decided to make the section analysis of the AFM images and obtained that the holes of the sample B are larger than those of sample A. In particular, the holes of sample B have double depth than those of sample A. Indeed, the total thickness of all the layers grown after the first QW is the double in sample B that in sample A. Thus, these results seem to be in agreement with our hypothesis.

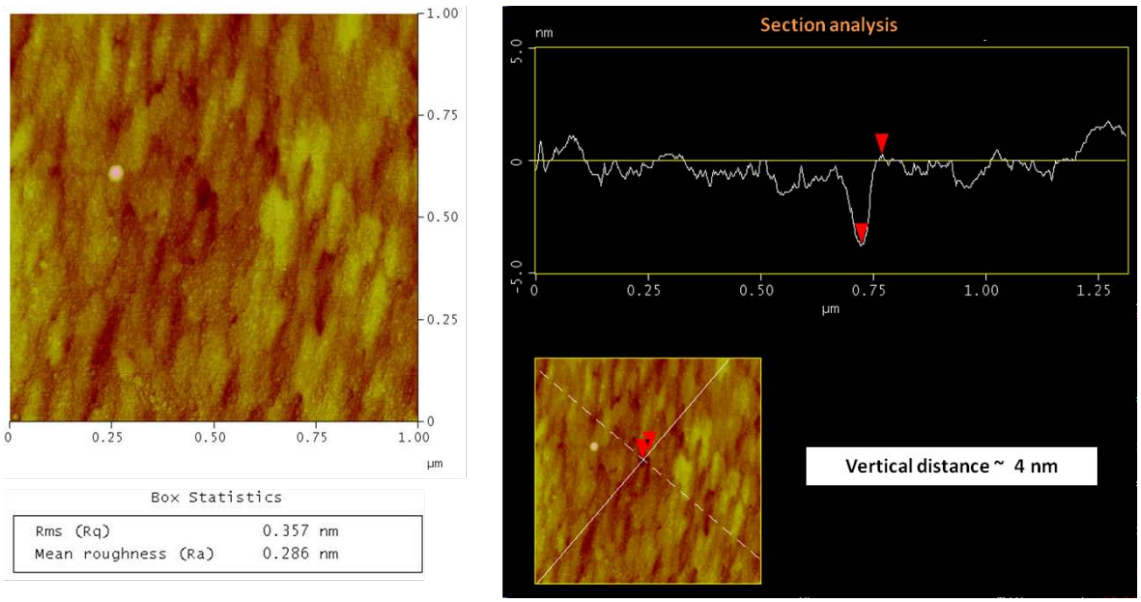

a) b)

Fig. 15 a) 1 x 1 µm AFM image and b) section analysis of the surface of the sample A after the fabrication process.

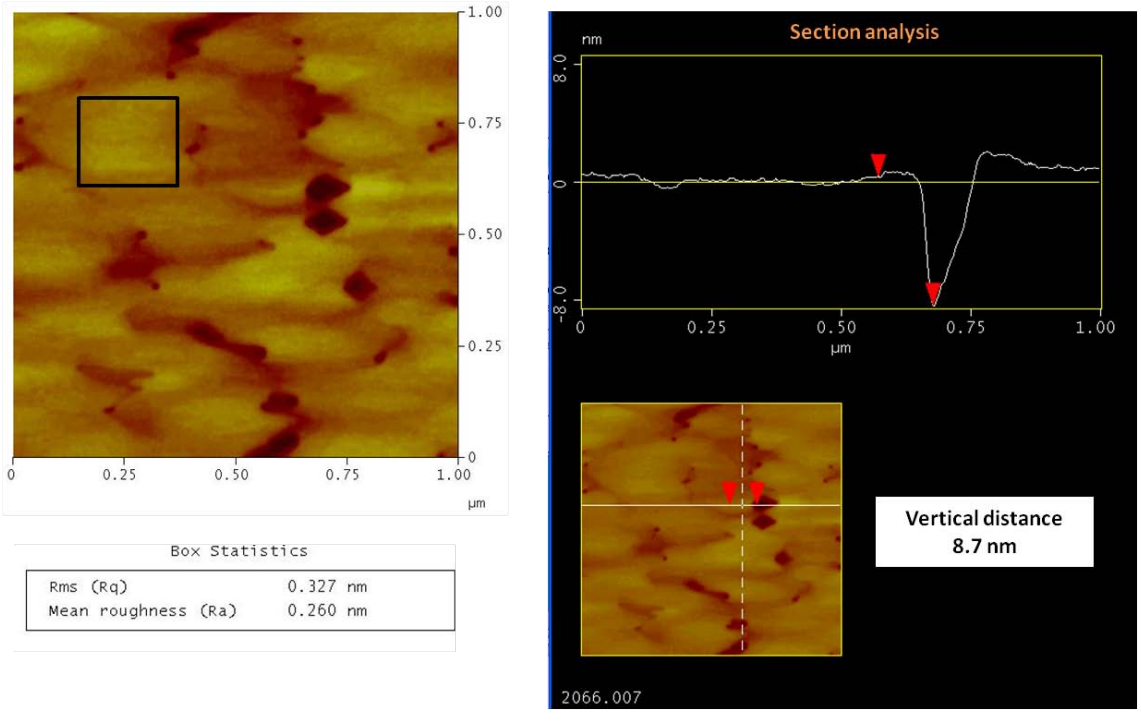

a) b)

Fig. 16 a) 1 x 1 µm AFM image and b) section analysis of the surface of the sample B after the fabrication process.

3.5 Fabrication and characterization of the IR photodetectors

3.5.1 Photodetector fabrication

Next, we processed the samples A and B as photodetectors (photodetector A and photodetector B, respectively). For this purpose, we cut a piece of sample of around 1 mm of width and deposited as lateral contacts two droplets of In at the position where QWs were etched using a soldering iron (see fig.17). Afterwards, this piece of sample was glued on a TO-8 with silver glue, and bonded by using gold wires for subsequent electrical measurements.

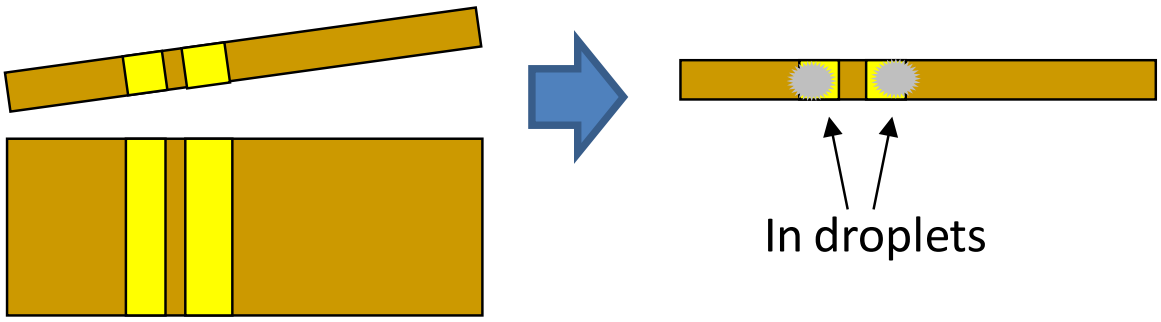

a)

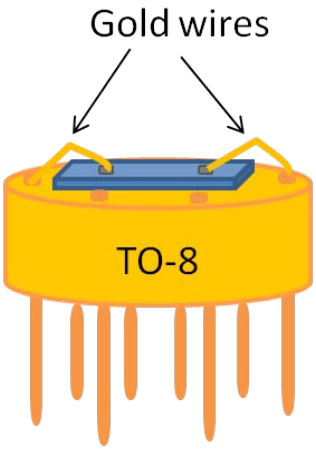

b)

Fig. 17 Processing of the sample as a photodetector: a) First, sample is cleaved,and ohmic contacts are deposited and second b) this piece of sample is glue on a TO-8 and gold wires are soldered to connect the contacts to the TO terminals.

3.5.2 I-V characterization

I-V characterization allows us to observe that the behavior of the contacts is clearly ohmic for both samples, and the value of the resistance between contacts is of order of hundreds of MΩ (fig. 18). This low conductivity of the photodetectors is in good agreement with the design of structure II, indicating that (a) despite the reduction of the barrier layers, there is no contact between QWs and (b) the edge of the QWs were completely etched (see fig. 19).

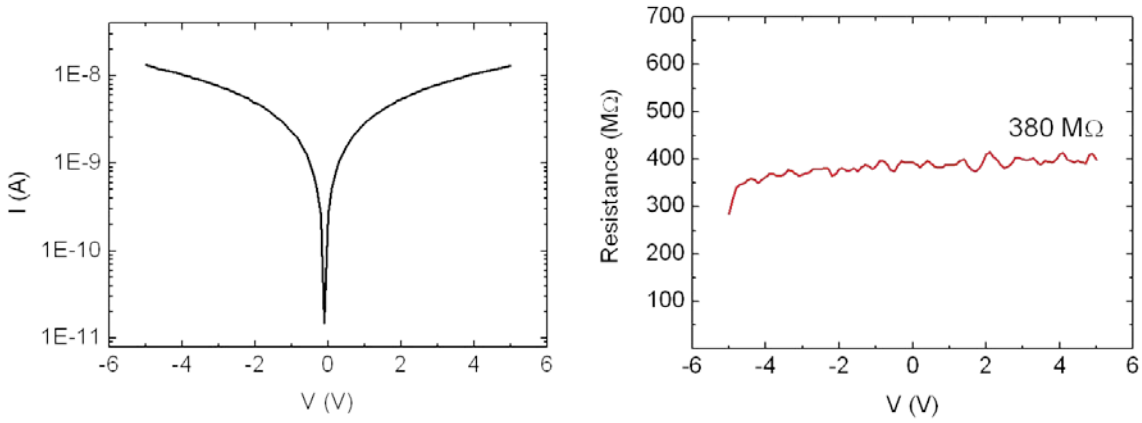

a)

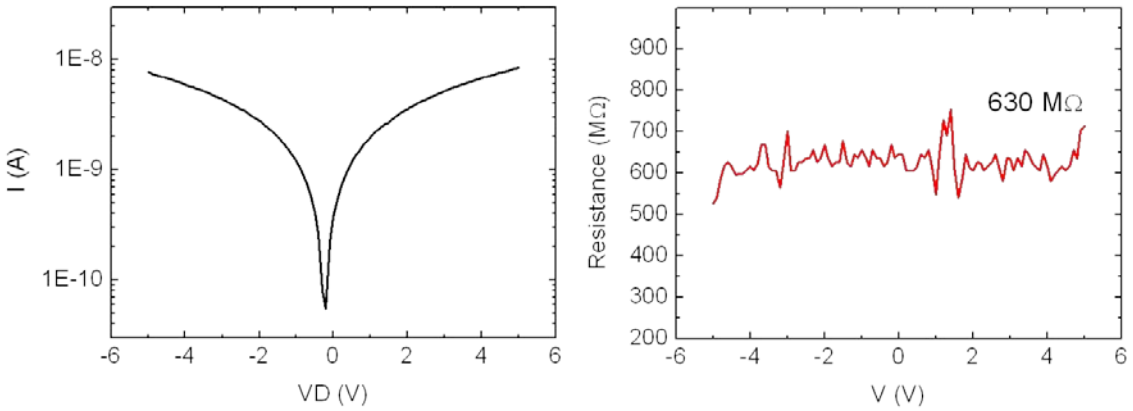

b)

Fig. 18 I-V characteristics and resistance as a function of the voltage of a) photodetector A and b) photodetector B.

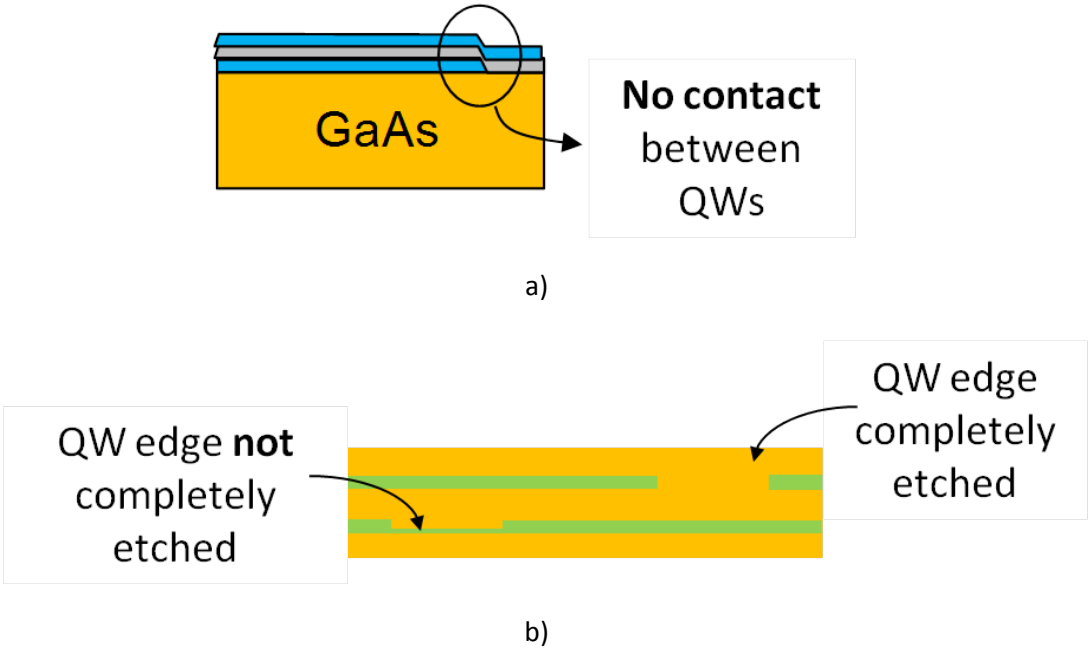

Fig. 19 a) Despite the reduction of the barriers, the samples fabricated have not contact between QWs. (b) Drawing of the possible problem in the etching of the QWs edges. In this case QW edges were completely etched

3.5.3 Fourier Transform Photocurrent Spectroscopy

Moreover, we measured the photocurrent spectrum of the two photodetectors fabricated using Fourier Transform (FT) Photocurrent Spectroscopy. This photocurrent technique consists of a photocurrent method in which monochromator is replaced by a Fourier Transform Infrared (FTIR) Spectrometer. FTIR allows to collect spectral data simultaneously in a wide spectral range, conferring a significant advantage over the dispersive spectrometer which studies one by one the individual wavelengths emitted from the light source [5]. Thus, advantages such as, speed, sensitivity, mechanical simplicity and self-calibration of the system lead us to replace the conventional dispersive spectrometer method by the FT Photocurrent Spectroscpy to carry out the characterization of the fabricated photodetectors.

In particular, the photocurrent spectrum measurements were performed using a Nicolet Magna-IR 760 with a KBr beam splitter and a glow bar source. The photodetector was placed inside an optical closed cycle He cryostat which allowed us to perform photocurrent measurements at very low temperatures, such as 15 K. In addition, we also measured the photocurrent using different bias voltages (Vb) applied between the ohmic contacts. The signal from the device was then amplified by a transimpedance amplifier and fed into the external detector port of the spectrometer. Fig. 20 shows the structure of the setup and electrical connections of the system built up in our lab.

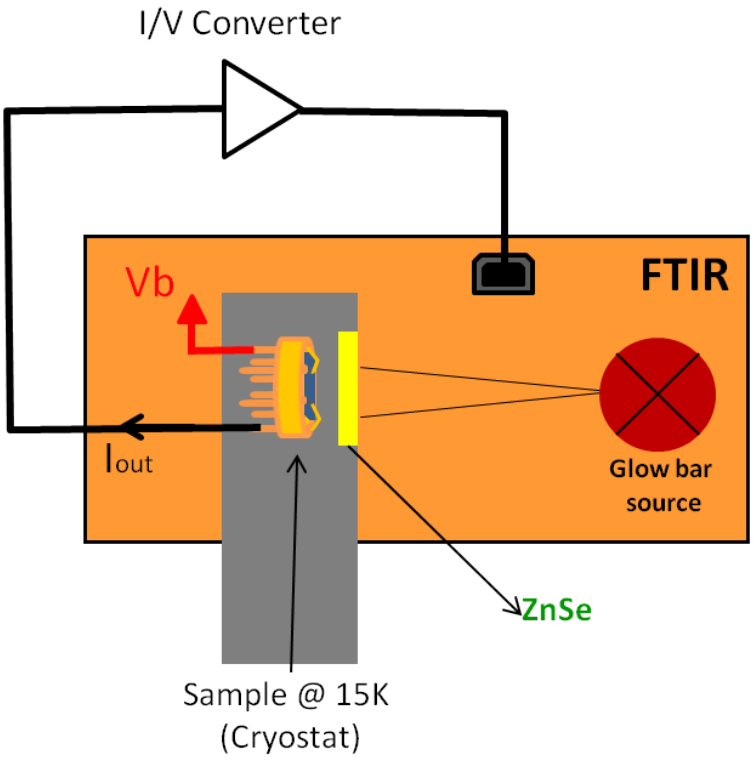

Fig. 20 FT Photocurrent Spectroscopy set-up and electrical connections of the system.

Scanning the spectrum from 0.9 to 40 µm at low temperatures, we found a clear detection band centered at 5 µm for both samples, A and B (see fig. 21).

Moreover, the intensity of the photocurrent depends on the bias voltage applied to the devices. As seen in fig. 21, the photoresponse increases with the absolute value of bias voltage in both cases. Nevertheless, each photodetector shows a different dependence on the polarity of this bias voltage. In the particular case of photodetector B, photoresponse show an asymmetric behavior about bias voltage of 0 V. While for negative Vb there is only a clear detection band at 5 µm, for positive Vb an additional band appears at lower wavelengths. Specifically, this new band is centered at 2 µm. On the other hand, photocurrent signal is higher for positive polarity. Nevertheless, for the photodetector A, negative polarities lead to higher photocurrent values than those obtained with positive bias voltages.

Additionally, as observed in photocurrent spectra, we demonstrate the operation of photovoltaic lateral bias IR photodetectors, since photodetectors are able to operate without the application of external bias voltage (i.e. in a photovoltaic mode).

Finally, photocurrent measurements were also carried out at room temperature. Unlike the results showed in the previous report, we found that the signal quenched above 15 K and is completely extinguished at room temperature. The design differences between the photodetector fabricated in that report and these ones are basically the thickness of both, QWs and barriers. In that case, the barrier thickness regrown on the bottom QW after the sputtered process was 10 and 20 times larger than that regrown for samples A and B,

respectively. Thus, the surface on which the top QW was grown may be of better structural quality than those of the sample A and B. As a consequence, this could give rise to the degradation of the photodetector performance.

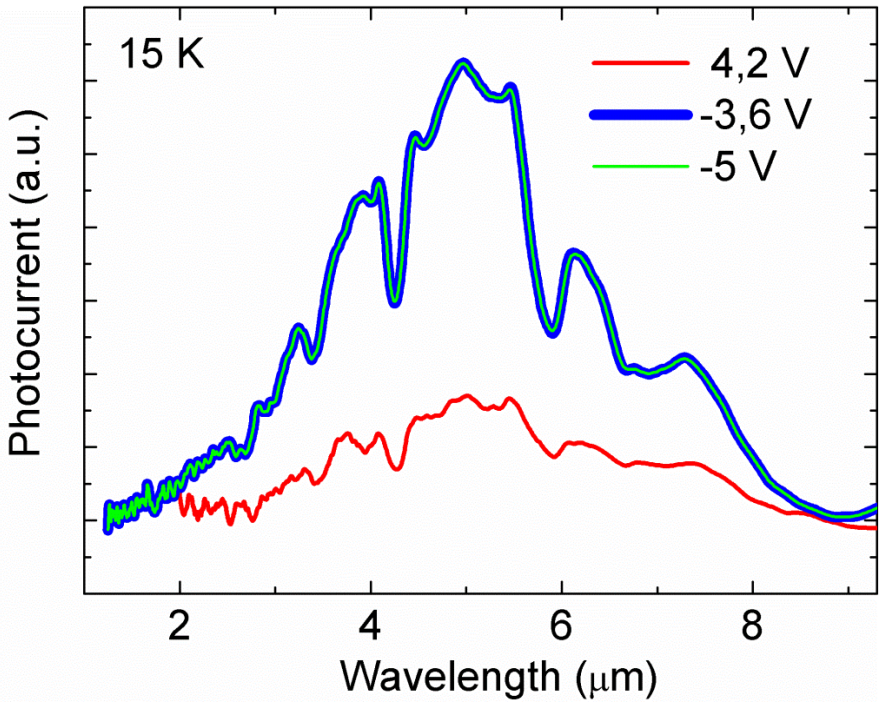

a)

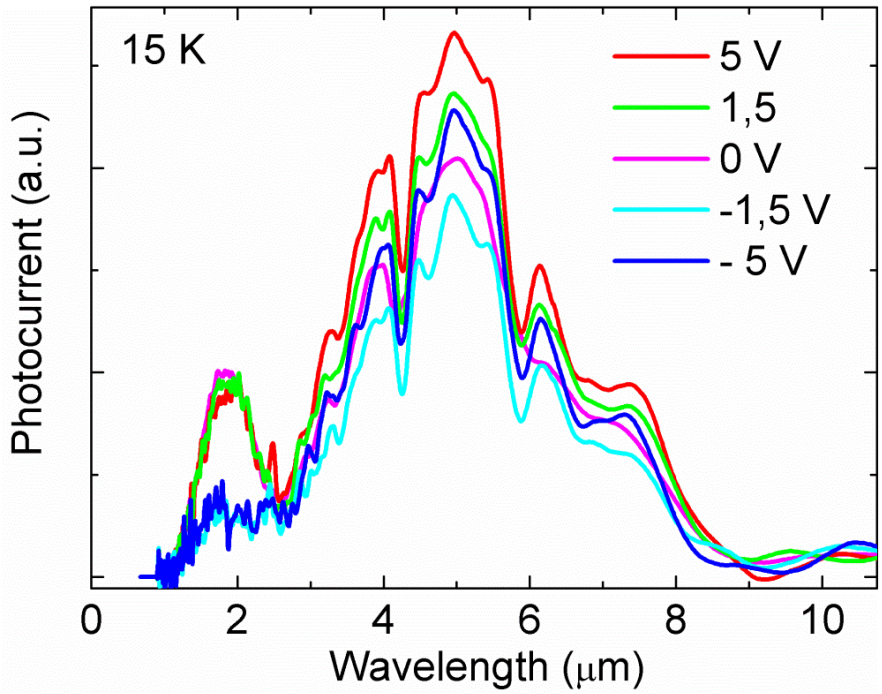

b)

Fig. 21 Photocurrent response spectra for a) sample A and b) sample B at different bias voltages. A main detection band is centered for both cases at 5 μm. An additional detection band centered at 2 μm is observed for sample B when positive bias voltages are applied.

As occurred at room temperature, we would expect that the I-V characteristic of the fabricated photodetectors is also symmetric at low temperatures (15K). By contrast, we found an asymmetric behavior of the I-V characteristic when this is measured at such a low temperatures. Fig. 22 show the I-V characteristic of photodetector B measured at room temperature and 15 K.

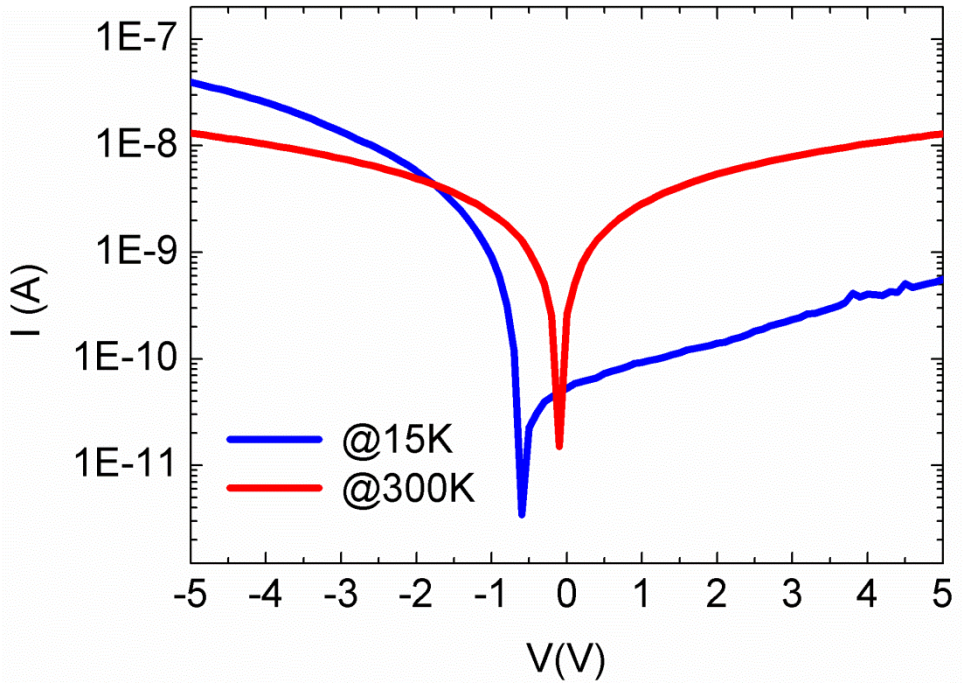

Fig. 22 I-V characteristic of photodetector B measured at 15 K and room temperature.

As already mentioned in this report, although bottom and top QWs are designed as equivalent layers (the same thickness, composition, doping and barriers), actually, they are not. In particular, the difference lies in the starting surface on which they are grown. While the bottom QW is grown on a "pure epitaxial surface" (without any kind of previous processing), the growth of the top QW is actually a regrowth process, since previously the sample underwent an etching process. This different nature of the QWs could explain the observed asymmetry of both photocurrent and I-V measurements. Additional experiments would need to be done in order to clarify this issue.

4 Final conclusions

The final conclusions of this report are the following:

- With respect to structure I
  - We improved the resist removal procedure after the ion implantation process adding an O_2 plasma etching step.
  - We obtained streaky RHEED patterns during the growth and better surface quality.
  - The samples were processed as photodetectors and high resistance values between lateral contacts were obtained.
  - Nomarski contrast images of the processed photodetectors revealed low quality of the surface.
  - Clearly, the optimization of the resist removal procedure needs to be done to develop structures of good quality.
- With respect to structure II
  - We have optimized the etching process to fulfill the structure II design requirements.
  - The morphological characterization by AFM of the etched surface using optimum etching conditions shows quality similar to that of the native substrate.
  - We have developed two samples with structure II reducing the QW/barrier thickness to 5/10 nm and 5/5 nm.
  - AFM images revealed that the crystal quality during the regrowth is decreased: formation of holes.
  - The samples were processed into photodetectors and encapsulated on a TO-8 to be characterized.
  - We obtained ohmic contacts and a high resistance between them demonstrating the total interruption of the QWs.
  - We built a Fourier Transform Photocurrent Spectroscopy set-up to perform the photoresponse characterization of the devices.
  - Low dark currents and a clear photocurrent band around 5 μm at 15 K were measured.
  - Photocurrent signal is extinguished at room temperature which could be related to the surface degradation of the structural quality after the etching process.
  - Photoresponse and I-V characteristics showed an asymmetric behavior with the polarity of the bias voltage. The different nature between QWs (top and bottom) could explain this asymmetry.
  - We demonstrated the operation of photovoltaic lateral bias IR photodetectors.

5 Final conclusions of the project

This project was aimed to the development of a suitable fabrication system to produce laterally-biased quantum well detectors with low dark current at room temperature. The main objectives can be summarized as follows:

1. Development of a ion beam etching chamber to be connected to the main MBE system. This objective was successfully achieved. A full chamber including vacuum pumps, ion beam source and Ar supply line was built and integrated with the main MBE chamber. The accuracy of the alternate etching steps is obtained by an external TV camera (to align different etching processes), and a complex control software for the ion beam fully developed at ISOM.

2. Optimization of the etching and post-growth processes in terms of surface quality. This goal has also been reached etching samples under different beam conditions (Ar flux, acceleration voltage, emission current, spot size or etching time).

3. Fabrication of structure I for RT operation. We have demonstrated RT response for MES-FET structures. With respect to JFET samples, it is still necessary to improve the technology processing. The complex design of the device makes difficult to remove completely the photoresist.

4. Fabrication of structure II for RT operation. The samples were fabricated by alternate etching and growth steps. The QW surface quality was demonstrated to be high enough, with RMS roughness similar to that of the bare substrates. They show IR response at low temperature, but even though the resistance of these samples are high, there is still a high dark current which avoids acquiring a clear photocurrent signal.

Further work is still necessary to improve the performance of the two structures. In particular, our current work is focused on the following items:

In previous reports we summarized the fabrication of the two structures mentioned in this report. We were able to obtain good RT response at 9 µm using a MES-FET scheme (structure I) to reduce dark current. It has been demonstrated that this technology is very promising for the development of single QWIP detectors working at high temperature.

Concerning structure II, it was difficult to obtain a degree of reproducibility and accuracy enough to ensure a RT operation of the samples. However, the experimental data reveal that (within the resolution of SEM), both QWs have been successfully etched at both sides. We think that the low thickness of the separating barrier could lead to the shortcircuit of both QW just at the edge of the etching region. This is not possible to be determined by structural characterization tools. Instead, a series of samples with different barrier thickness should be grown, processed, encapsulated and measured. This work is currently in progress.

In summary we sincerely think that the work realized within these two years have been very successful. As a result, 1 publication and 1 presentation in an international congress were obtained [2] [6].

6 References

[1] P.M. Alsing, D.A. Cardimona, D.H. Huang, T. Apostolova, W.R. Glass, C.D. Castillo, Infrared Physics & Technology 50 (2007) 89–94.

[2] Álvaro Guzmán, Rocío San-Román, Adrián Hierro, Journal of Crystal Growth 323, (2011), 496-500.

[3] Semiconductor Devices: Physics and Technology 2nd Ed., S.M. Sze, John Wiley and sons, Inc.

[4] Cold Plasma in Materials Fabrication, Alfred Grill, IEEE Press, 1993.

[5] http://mmrc.caltech.edu/FTIR/FTIRintro.pdf

[6] "Laterally biased double quantum well IR detector fabricated by MBE regrowth", Álvaro Guzmán, Rocío San-Román, Adrián Hierro, 16th International Conference on Molecular Beam Epitaxy, Berlín (Germany), 22-27 August 2010.

7 List of symbols, abbreviations and acronyms

AFM	Atomic Force Microscope
MBE	Molecular Beam Epitaxy
QW	Quantum Well
SEM	Scanning Electron Microscope
Structure I	Summarized in fig. 1
Structure II	Summarized in fig. 1
Vb	Bias voltage
μ	Electron mobility
R	Resistance
RHEED	Reflection High Energy Electron Diffraction
RT	Room Temperature